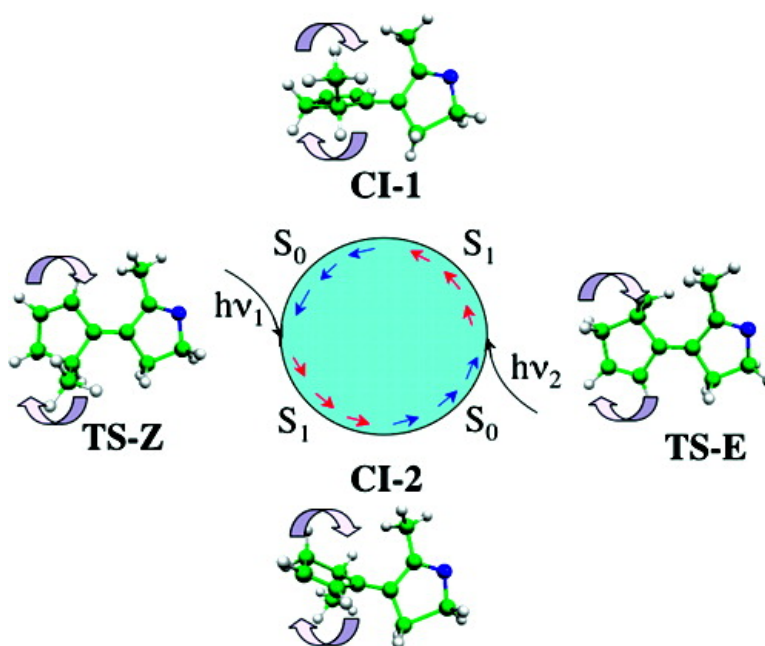Article

Design and Photochemical Characterization of a Biomimetic Light-Driven Z/E Switcher

Diego Sampedro, Annapaola Migani, Alessandra Pepi, Elena Busi, Riccardo Basosi, Loredana Latterini, Fausto Elisei, Stefania Fusi, Fabio Ponticelli, Vinicio Zanirato, and Massimo Olivucci

More About This Article

Additional resources and features associated with this article are available within the HTML version:

- Supporting Information
- Access to high resolution figures
- Links to articles and content related to this article
- Copyright permission to reproduce figures and/or text from this article

View the Full Text HTML

Design and Photochemical Characterization of a Biomimetic Light-Driven Z/E Switcher

Diego Sampedro,[†] Annapaola Migani,[†] Alessandra Pepi,[†] Elena Busi,[†]
Riccardo Basosi,[†,‡] Loredana Latterini,[||] Fausto Elisei,[||] Stefania Fusi,[†]
Fabio Ponticelli,[†] Vinicio Zanirato*,[§] and Massimo Olivucci*,[†,‡]

*Contribution from the Dipartimento di Chimica, Università di Siena, Via Aldo Moro 2,
I-53100 Siena, Italy, Centro di Studio dei Sistemi Complessi, Via Tommaso Pendola 37,
I-53100 Siena, Italy, Dipartimento di Scienze Farmaceutiche, Università di Ferrara,
Via Fossato di Mortara 17−19, I-44100 Ferrara, Italy, and Dipartimento di Chimica,
Laboratorio di Chimica Fisica, Via Elce di Sotto 8, I-06123 Perugia, Italy*

Received October 3, 2003; E-mail: olivucci@unisi.it; znv@dns.unife.it

Abstract: Protonated Schiff bases (PSBs) of polyenals constitute a class of light-driven switchers selected by biological evolution that provide model compounds for the development of artificial light-driven molecular devices or motors. In the present paper, our primary target is to show, through combined computational and experimental studies, that it is possible to approach the design of artificial PSBs suitable for such applications. Below, we use the methods of computational photochemistry to design and characterize the prototype biomimetic molecular switchers 4-cyclopenten-2′-enylidene-3,4-dihydro-2H-pyrrolinium and its 5,5′-dimethyl derivative both containing the penta-2,4-dieniminium chromophore. To find support for the predicted behavior, we also report the photochemical reaction path of the synthetically accessible compound 4-benzylidene-3,4-dihydro-2*H*-pyrrolinium. We show that the preparation and photochemical characterization of this compound (together with three different *N*-methyl derivatives) provide both support for the predicted photoisomerization mechanism and information on its sensitivity to the molecular environment.

1. Introduction

Molecular switchers based on photochemical E/Z isomerization have been employed in different contexts to convert light-energy into "mechanical" motion at the molecular level.[1,2] In basically all applications, the induced motion results in a permanent or transient conformational change of a molecular scaffold bounded to the switcher. Using this simple principle, switchers based on the azobenzene chromophore have been used to control properties such as ion complexation,[3,4] electronic properties[5] and catalysis[6] or to trigger folding/unfolding of oligopeptide chains.[7−12] A particularly sophisticated application

of the above principle is the construction of single molecules capable to convert light-energy in continuous unidirectional rotary motion. Indeed, it has been shown that photochemical E/Z switchers corresponding to chiral diarylidenes constitute examples of light-driven molecular rotors.[13−16] Here, the spatial asymmetry (i.e., the chirality) of the molecular framework determines the direction (either clockwise or counterclockwise) of the E → Z and Z → E conformational changes leading, after sequential absorption of two photons, to a complete (360°) rotation.

Chiral E/Z switchers are also known in photobiology. For instance, the retinal chromophore of rhodopsin proteins,[17−19] a large class of trans-membrane photoreceptors, undergoes an efficient unidirectional photoisomerization that, ultimately, triggers a conformational change of the native protein scaffold.

† Dipartimento di Chimica, Università di Siena.
‡ Centro di Studio dei Sistemi Complessi.
§ Dipartimento di Scienze Farmaceutiche, Università di Ferrara.
|| Dipartimento di Chimica, Laboratorio di Chimica Fisica.

(1) Sauvage, J.-P., Ed.; *Molecular Machines and Motors*; Springer-Verlag: Berlin, London, 2001; Vol. 99.
(2) Drexler, K. E. *Nanosystems: Molecular Machinery, Manufacturing and Computation*; John Wiley & Sons: New York, 1992.
(3) Shinkai, S.; Kusano, Y.; Manabe, O.; Nakaji, T.; Nishida, Y.; Ogawa, T. *J. Am. Chem. Soc.* **1980**, *102*, 5860−5865.
(4) Shinkai, S.; Minami, T.; Kusano, Y.; Manabe, O. *J. Am. Chem. Soc.* **1983**, *105*, 1851−1856.
(5) Jousselme, B.; Blanchard, P.; Gallego-Planas, N.; Delaunay, J.; Allain, M.; Richomme, P.; Levillain, E.; Roncali, J. *J. Am. Chem. Soc.* **2003**, *125*, 2888−2889.
(6) Cacciapaglia, R.; Stefano, S. D.; Mandolini, L. *J. Am. Chem. Soc.* **2003**, *125*, 2224−2227.
(7) Behrendt, R.; Renner, C.; Schenk, M.; Wang, F.; Wachtveitl, J.; Oesterhelt, D.; Moroder, L. *Angew. Chem., Int. Ed. Engl.* **1999**, *38*, 2771−2774.
(8) Bredenbeck, J.; Helbing, J.; Sieg, A.; Schrader, T.; Zinth, W.; Renner, C.; Behrendt, R.; Moroder, L.; Wachtveitl, J.; Hamm, P. *Proc. Natl. Acad. Sci. U.S.A.* **2003**.
(9) Ulysse, L.; Cubillos, J.; Chmielewski, J. *J. Am. Chem. Soc.* **1995**, *117*, 8466−8467.
(10) Rudolph-Böhner, S.; Krüger, M.; Oesterhelt, D.; Moroder, L.; Nägele, T.; Wachtveitl, J. *J. Photochem. Photobiol. A* **1997**, *105*, 235−248.
(11) Renner, C.; Behrendt, R.; Spörlein, S.; Wachtveitl, J.; Moroder, L. *Biopolymers* **2000**, *54*, 489−500.
(12) Spörlein, S.; Carstens, H.; Satzger, H.; Renner, C.; Behrendt, R.; Moroder, L.; Tavan, P.; Zinth, W.; Wachtveitl, J. *Proc. Natl. Acad. Sci. U.S.A.* **2002**, *99*, 7998−8002.
(13) Koumura, N.; Geertsema, E. M.; van Gelder, M. B.; Meetsma, A.; Feringa, B. L. *J. Am. Chem. Soc.* **2002**, *124*, 5037−5051.
(14) Koumura, N.; Zijistra, R. W. J.; van Delden, R. A.; Harada, N.; Feringa, B. L. *Nature* **1999**, *401*, 152−155.
(15) Koumura, N.; Geertsema, E. M.; Meetsma, A.; Feringa, B. L. *J. Am. Chem. Soc.* **2000**, *122*, 12 005−12 006.
(16) Feringa, B. L. *Acc. Chem. Res.* **2001**, *34*, 504−516.
(17) Mathies, R. A.; Lugtenburg, J. In *Handbook of Biological Physics*; Stavenga, D. G., de Grip, W. J., Pugh, E. N., Eds.; Elsevier Science: New York, 2000; Vol. 3, pp 56−90.
(18) Kandori, H.; Shichida, Y.; Yoshizawa, T. *Biochemistry (Moscow)* **2001**, *66*, 1483−1498.
(19) Teller, D. C.; Okada, T.; Behnke, C. A.; Palczewski, K.; Stenkamp, R. E. *Biochemistry* **2001**, *40*, 7761−7772.

Scheme 1

(a)   (b)

Scheme 2
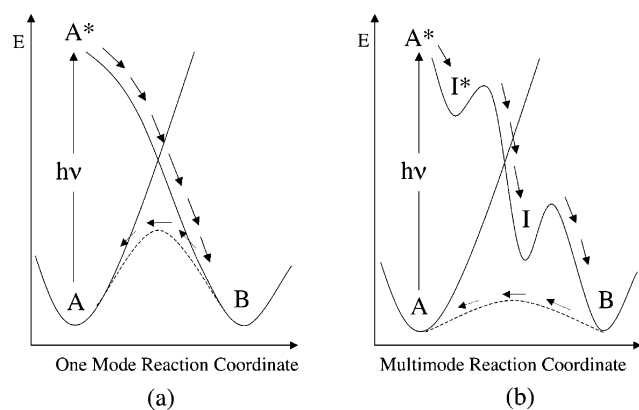
In rhodopsin (Rh) itself (i.e., the visual receptor of superior animals) the photoisomerization of the native 11-*cis*-retinal chromophore (PSB11) to its all-trans form occurs with a 0.67 quantum yield.[20] This value is larger than the 0.25 value measured for the same chromophore in ethanol solution[21,22] and also larger than the 0.28 and 0.51 values measured for the photoisomerization of *trans*- and *cis*-azobenzene, respectively.[23] Due to its high photoisomerization efficiency, bacteriorhodopsin (a member of the same photoreceptor family) and its mutants, have been exploited to produce different light-driven molecular devices (see ref 24 and references therein).
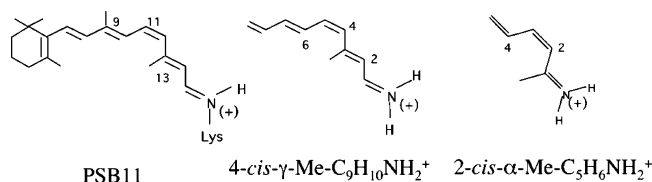
It is apparent that the efficiency of the Z/E isomerization of Rh must depend on the structure of the associated reaction path. This idea is illustrated in Scheme 1 where a model reaction path for an efficient (Scheme 1a) and a less efficient (Scheme 1b) switcher is reported. Accordingly, an efficient photoisomerization would occur when the photoexcited reactant A* evolves along a barrierless excited-state path, decays at a *real* surface crossing (a conical intersection, **CI**)[25,26] and finally relaxes to the energy minimum corresponding to photoproduct B. Furthermore, in an efficient switcher, the reaction coordinate connecting A* to B should be as simple as possible i.e., dominated only by the *reactive* mode (e.g., the isomerization mode) or by modes strongly coupled to it. As we will discuss below, such a coordinate helps to limit the wastage of the photon energy that has to be *converted* to reactive motion and *not redistributed* among the remaining $3N - 7$ internal degrees of freedom of the system (here, N indicates the number of atoms of A). In contrast, the reaction path of Scheme 1b belongs to an inefficient switcher. In fact, the presence of excited state and/or ground-state intermediates (I* and I respectively) along
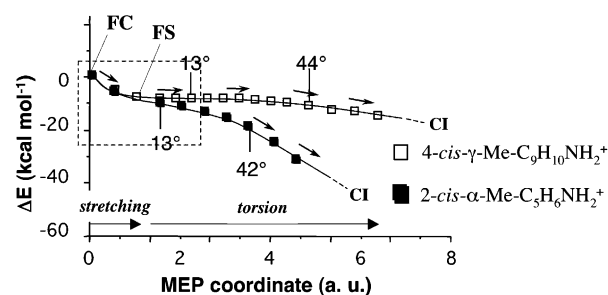
the path allows for redistribution of the photon energy. An additional desirable property of photochemical switchers is the stability of the isomers A and B with respect to thermal (i.e., ground state) Z/E isomerization. As shown in Scheme 1a (see dashed energy profile), in an efficient switcher the barrier for thermal Z/E isomerization must be high enough to restrain the return of B to A.

The ultrafast 200 fs reaction time scale[27,28] and vibrational coherence[28] observed for the photoisomerization of PSB11 in Rh, suggest that the reaction occurs via the mechanism shown in Scheme 1a. In this model, the quantum yield of the reaction and the nuclear velocity along the reaction coordinate must be related by the Landau−Zener formula.[29] The high quantum yield is thus a consequence of the high rate of the 11-cis → all-trans isomerization.[17,28,30] This idea is supported by the fact that 13-demethyl-Rh (an isomer of Rh where the 13-methyl group of PSB11 has been removed) and isorhodopsin (an isomer of Rh containing a 9-*cis* retinal chromophore) isomerize more slowly[30,31] and have lower quantum yields[32,33] than Rh.

PSB11 corresponds to the protonated Schiff base (PSB) of a polyenal. The primary target of the present paper is to show, through combined computational and experimental studies, that certain biomimetic PSBs provide suitable "frameworks" for the design of molecular switchers or motors. In the past, retinal PSB models have been the subject of several computational studies.[34−44] The first example is provided by the PSB11 model 4-*cis*-γ-methylnona-2,4,6,8-tetra-enimminium (4-cis-γ-Me-C_9H_{10}-NH_2^+). As reported in Scheme 2, the S_1 isomerization path of this molecule is sequentially dominated by two very different

(20) Dartnall, H. *Visio Res.* **1967**, *8*, 339−358.
(21) Becker, R. S. *Photochem. Photobiol.* **1988**, *48*, 369−399.
(22) Becker, R. S.; Freedman, K. A. *J. Am. Chem. Soc.* **1985**, *107*, 1477−1485.
(23) Bortolus, P.; Monti, S. *J. Phys. Chem.* **1979**, *83*, 648−652.
(24) Birge, R. R.; Gillespie, N. B.; Izaguirre, E. W.; KUsnetzow, A.; Lawrence, A. F.; Singh, D.; Song, W.; Schmidt, E.; Stuart, J. A.; Seetharaman, S.; Wise, K. J. *J. Phys. Chem. B* **1999**, *103*, 10 746−10 766.
(25) Bernardi, F.; Olivucci, M.; Robb, M. A. *Chem. Soc. Rev.* **1996**, 321−328.
(26) Michl, J.; Bonacic-Koutecky, V. *Electronic Aspects of Organic Photochemistry*; Wiley: New York, 1990.

(27) Schoenlein, R. W.; Peteanu, L. A.; Mathies, R. A.; Shank, C. V. *Science* **1991**, *254*, 412−415.
(28) Wang, Q.; Schoenlein, R. W.; Peteanu, L. A.; Mathies, R. A.; Shank, C. V. *Science* **1994**, *266*, 422−424.
(29) Desouter-Lecomte, M.; Lorquet, J. C. *J. Chem. Phys.* **1979**, *71*, 3661−3672.
(30) Wang, Q.; Kochendoerfer, G. G.; Schoenlein, R. W.; Verdegem, P. J. E.; Lugtenburg, J.; Mathies, R. A.; Shank, C. V. *J. Phys. Chem.* **1996**, *100*, 17 388−17 394.
(31) Schoenlein, R. W.; Peteanu, L. A.; Wang, Q.; Mathies, R. A.; Shank, C. V. *J. Phys. Chem.* **1993**, *97*, 12 087−12 092.
(32) DeLange, F.; Bovee-Geurts, P. H. M.; Van Oostrum, J.; Daniel Portier, M.; Verdegem, P. J. E.; Lugtenburg, J.; de Grip, W. J. *Biochem.* **1999**, *37*, 1411−1420.
(33) Hurley, J.; Ebrey, T.; Honig, B.; Ottolenghi, M. *Nature (London)* **1977**, *270*, 540−542.
(34) Ben-Nun, M.; Molnar, F.; Schulten, K.; Martinez, T. J. *Proc. Natl. Acad. Sci. U.S.A.* **2002**, *99*, 1769−1773.
(35) Nonella, M. *J. Phys. Chem. B* **2000**, *104*, 11 379−11 388.
(36) Bonacic-Koutecky, V.; Köhler, K.; Michl, J. *Chem. Phys. Lett.* **1984**, *104*, 440−443.
(37) Bonacic-Koutecky, V.; Köhler, K.; Michl, J. *Angew. Chem., Int. Ed.* **1987**, *26*, 170−189.
(38) Tajkhorshid, E.; Suhai, S. *J. Phys. Chem. B* **1999**, *103*, 5581−5590.
(39) Birge, R. R.; Hubbard, L. M. *J. Am. Chem. Soc.* **1980**, *102*, 2195−2205.
(40) Weingart, O.; Buss, V. *Phase Trans.* **2001**, *75*, 19−29.
(41) Warshel, A. *Nature* **1976**, *260*, 769−683.
(42) Grossjean, M. F.; Tavan, P.; Schulten, K. *J. Phys. Chem.* **1990**, *94*, 8059−8069.

Scheme 3
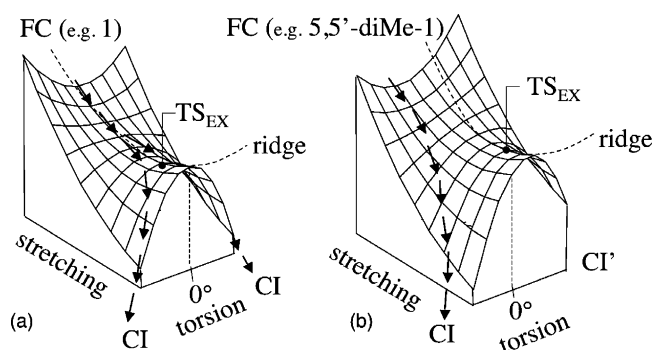
molecular modes.[45] The first describes the initial relaxation from the Franck−Condon (**FC**) point to a planar intermediate **FS** and is dominated by a double-bond-expansion/single-bond-contraction (i.e., stretching) mode. In contrast, the second mode describes the evolution of **FS** along the 4-cis→all-trans isomerization mode ultimately leading to decay through a conical intersection (**CI**). Since the **FC → FS** relaxation is substantially uncoupled to the isomerization, **FS** can be associated to I* of Scheme 1a. Accordingly, the kinetic energy gained during the initial relaxation may not be efficiently converted into Z → E motion.
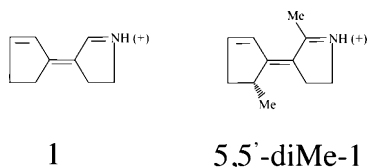
Isomerization path computations for the 2-*cis*-α-methyl-penta-2,4-dieniminium (2-*cis*-α-Me−$C_5H_6NH_2^+$), a minimal model of PSB11 with a penta-2,4-dieniminium ($-CH=CH-CH=CH-CH=NH(+)-$) moiety, indicate that this system provides a more suitable backbone.[43,46] Indeed, such path shows no flat S_1 energy plateau (see framed region in Scheme 2) and the shape of the potential energy surface corresponds to that given in Scheme 3a. Due to the highly anharmonic shape of the S_1 energy surface, the barrierless path of 2-*cis*-α-Me−$C_5H_6NH_2^+$ (see stream of arrows in Scheme 3a) is driven by highly coupled stretching and isomerization modes. Thus, the reaction coordinate becomes, to a certain extent, closer to the single-mode coordinate of Scheme 1a, where one expects limited energy redistribution and fast isomerization. This conclusion is supported by semiclassical dynamics computations that predict that 2-cis-α-Me−$C_5H_6NH_2^+$ isomerizes in less than 100 fs.[47]
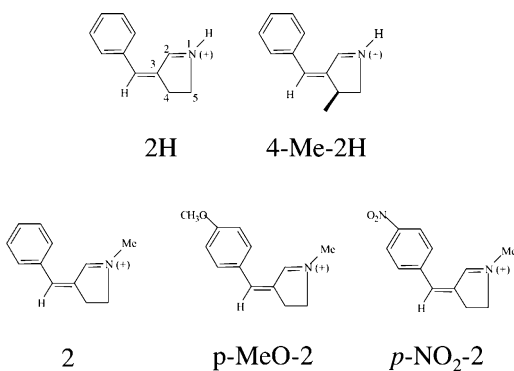
To the best of our knowledge, attempts to synthesize compounds containing the penta-2,4-dieniminium biomimetic backbone have never been reported. As a consequence, their synthesis represents an attractive target. Below, we apply the methods of computational photochemistry[48,49] to characterize the prototype molecular switcher 4-cyclopenten-2′-enylidene-3,4-dihydro-2H-pyrrolinium (**1**) and molecular rotor 5-methyl-4-(5′-methylcyclopent-2′-enylidene)-3,4-dihydro-2H-pyrrolinium (5,5′-diMe-**1**) both containing the penta-2,4-dieniminium unit. To find support for our predictions we also report the computation of the photochemical reaction path of the synthetically accessible structure 4-benzylidene-3,4-dihydro-2*H*-pyrrolium (**2H**) where the terminal C=C double-bond of the penta-2,4-dieniminium unit is replaced with a phenyl. We show that the photochemical characterization of **2H** (together with its derivatives 4-Me-**2H**, **2**, *p*-MeO-**2**, *p*-NO₂-**2**) provide support for the predicted photoisomerization mechanism and sensitivity to the molecular environment.

2. Experimental and Computational Methods

2.1 Computational Methods. The photoisomerization paths of *E*-**2H** have been determined using fully unconstrained ab initio quantum chemical computations in the framework of a CASPT2//CASSCF strategy.[33,34] This requires that the reaction coordinate is computed at the complete active space self-consistent field (CASSCF) level of theory and that the corresponding energy profile is re-evaluated at the multiconfigurational second-order Moller−Plesset perturbation theory level (here we used the CASPT2 method implemented in MOLCAS-5)[50] to take into account the effect of electron dynamic correlation. This approach allows for an accurate evaluation of excited-state energy barriers.[51] Thus, for **1**, 5,5′-diMe-**1** and *E*-**2H** the photoisomerization coordinate is determined via CASSCF minimum energy path (MEP) computations in mass-weighted Cartesians, whereas an S_1 single-bond twisting path (see subsection 3.4.3) was built by linear interpolation of CASSCF optimized geometries.

For the CASPT2 calculations we used a zeroth-order three-root (S_0, S_1, S_2) state-average CASSCF wave function characterized by a complete active space of 10-electrons in 10-orbitals (10e/10o). For the CASPT2 computations of **1** and 5,5′-diMe-**1** we used a zero-order two-root (S_0, S_1) state-average wave function with a 6e/6o complete active space. The CASPT2

(43) Garavelli, M.; Celani, P.; Bernardi, F.; Robb, M. A.; Olivucci, M. *J. Am. Chem. Soc.* **1997**, *119*, 6891−6901.
(44) Gonzales-Luque, R.; Garavelli, M.; Bernardi, F.; Merchan, M.; Robb, M. A.; Olivucci, M. *Proc. Natl. Acad. Sci. U.S.A.* **2000**, *97*, 9379−9384.
(45) Garavelli, M.; Vreven, T.; Celani, P.; Bernardi, F.; Robb, M. A.; Olivucci, M. *J. Am. Chem. Soc.* **1998**, *120*, 1285−1288.
(46) Garavelli, M.; Bernardi, F.; Olivucci, M.; Vreven, T.; Klein, S.; Celani, P.; Robb, M. A. *Faraday Discuss.* **1998**, *110*, 1−20.
(47) Vreven, T.; Bernardi, F.; Garavelli, M.; Olivucci, M.; Robb, M. A.; Schlegel, H. B. *J. Am. Chem. Soc.* **1977**, *119*, 12 687−12 688.
(48) Olivucci, M.; Robb, M. A.; Bernardi, F. In *Conformational Analysis of Molecules in Excited States*; Waluk, J., Ed.; Wiley-VCH: John Wiley and Sons Inc.: New York, 2000; pp 297−366.
(49) Robb, M. A.; Garavelli, M.; Olivucci, M.; Bernardi, F. In *Reviews in Computational Chemistry*; Lipkowitz, K. B., Boyd, D. B., Ed.; Wiley-VCH: John Wiley and Sons Inc.: New York, Chichester, 2000; pp 87−146.
(50) Andersson, K.; Barisz, M.; Bernhardsson, A.; Blomberg, M. R. A.; Cooper, D. L.; Fleig, T.; Fülscher, M, P.; de Graaf, C.; Hess, B. A.; Karlström, G.; Lindh, R.; Malmqvist, P.-Å.; Neogrády, P.; Olsen, J.; Roos, B. O.; Schmmelpfennid, B.; Schültz, M.; Sadlej, A. J.; Schütz, M.; Seijo, L.; Serrano-Andrés, L.; Siegbahn, P. E. M.; Stårling, T.; Thorsteinsson, T.; Veryazov, V.; Widmark, P.-O.; version 5.1 ed.: University of Lund, Sweden, 2000.
(51) Page, C. S.; Olivucci, M. *J. Comput. Chem.* **2003**, *24*, 298−309.

correction was applied only to CASSCF optimized geometries (minima, transition states, and conical intersections). A detailed comparison between the CASSCF and CASPT2 energy profiles, absolute and relative energies for **1**, 5,5′-diMe-**1** and *E*-**2H** can be found in the Supporting Information.

In all of the CASSCF and CASPT2 calculations we employed the 6-31G* basis set except when otherwise stated. The S_2 state of the penta-2,4-dieniminium cation has been found to lie well above (~30 kcal mol^{-1}) the lowest S_1 state.[43] For this reason, the S_2 state is expected not to contribute to the photocycle of **1** and 5,5′-diMe-**1** and therefore is not considered. For comparison with the experimental absorption spectrum the vertical excitation energies for compound *E*-**2H** were computed at the CASPT2 level for the three lowest singlet excited states by averaging four roots (ground state and three excited states). To assess the effect of basis set expansion, the CASPT2 calculations at **FC** were repeated using the 6-31G** basis set.

The molecular dipole moments and charge distribution (Mulliken charges) along the backbone of *E*-**2H** are determined at the CASSCF level of theory (see Supporting Information for details). The structure of all conical intersections have been optimized applying the methodology included in GAUSSIAN 98.[52] The initial relaxation direction (IRD) method[53,54] was used to locate the steepest-descent direction to be follow in the MEP calculation when starting at **FC** or **CI** points.

2.2 Synthesis and Photochemical Studies. The E- and Z-isomers of **2**, *p*-MeO-**2**, *p*-NO$_2$-**2** were easily obtained starting from the corresponding neutral imines. Because the *E*-stereoisomers are largely predominant in the synthesized neutral forms **2neut**, *p*-MeO-**2neut**, *p*-NO$_2$-**2neut**, the corresponding Z-stereoisomers were obtained through irradiation of the E form. The two isomers could be separated by chromatography. While reaction of the E- and Z-stereoisomers of **2neut**, *p*-MeO-**2neut**, and *p*-NO$_2$-**2neut** with trifluoroacetic acid yielded the corresponding PSBs, the reaction with methyl trifluoromethanesulfonate led quantitatively to the formation of the E- and Z-forms of **2**, *p*-MeO-**2**, and *p*-NO$_2$-**2**. These methylated derivatives were found to be more stable and tractable than the protonated forms. In particular, we observed that the protonated Z-stereoisomers (**2H**, *p*-MeO-**2H**, and *p*-NO$_2$-**2H**) tended to transform thermally to the corresponding E-stereoisomers in the presence of impurities. The higher stability of *N*-methyl compounds is qualitatively rationalized by the additional stabilization of the positive charge at *N* and by the decreased mobility of the alkyl group with respect to the proton. Full synthetic procedures and characterization of new compounds are reported in the Supporting Information.

(52) Frisch, M. J.; Trucks, G. W.; Schlegel, H. B.; Scuseria, G. E.; Robb, M. A.; Cheeseman, J. R.; Zakrzewski, V. G.; Montgomery, J. A., Jr.; Stratmann, R. E.; Burant, J. C.; Dapprich, S.; Millam, J. M.; Daniels, A. D.; Kudin, K. N.; Strain, M. C.; Farkas, O.; Tomasi, J.; Barone, V.; Cossi, M.; Cammi, R.; Mennucci, B.; Pomelli, C.; Adamo, C.; Clifford, S.; Ochterski, J.; Petersson, G. A.; Ayala, P. Y.; Cui, Q.; Morokuma, K.; Malick, D. K.; Rabuck, A. D.; Raghavachari, K.; Foresman, J. B.; Cioslowski, J.; Ortiz, J. V.; Stefanov, B. B.; Liu, G.; Liashenko, A.; Piskorz, P.; Komaromi, I.; Gomperts, R.; Martin, R. L.; Fox, D. J.; Keith, T.; Al-Laham, M. A.; Peng, C. Y.; Nanayakkara, A.; Gonzalez, C.; Challacombe, M.; Gill, P. M. W.; Johnson, B. G.; Chen, W.; Wong, M. W.; Andres, J. L.; Head-Gordon, M.; Replogle, E. S.; Pople, J. A. *Gaussian 98*, revision A.7; Gaussian, Inc.: Pittsburgh, PA, 1998.
(53) Celani, O.; Robb, M. A.; Garavelli, M.; Bernardi, F.; Olivucci, M. *Chem. Phys. Lett.* **1995**, *243*, 1−8.
(54) Garavelli, M.; Celani, P.; Fato, M.; Bearpark, M. J.; Smith, B. R.; Olivucci, M.; Robb, M. A. *J. Phys. Chem. A* **1997**, *101*, 2023−2032.

3. Results and Discussion

In subsection 3.1, we report the computed photochemical and thermal reaction paths driving the isomerization of the E- and Z- forms of **1**. To investigate the possibility of prompting unidirectional rotary motion, in subsection 3.2 we compare the structure of the energy surface of **1** with that of its chiral derivative 5,5′-diMe-**1**. In subsection 3.3, we demonstrate that the photochemical reaction path of the synthetically accessible chromophore **2H** conforms to that seen for **1**. Finally, in subsection 3.4, we report the synthesis and the experimental characterization of the derivatives **2**, *p*-MeO-**2**, and *p*-NO$_2$-**2**. Unless otherwise stated, we shall only discuss CASPT2 energies. Reaction paths are structural features of the potential energy surface and do not provide direct information on the molecular motion. However, since trajectory or quantum dynamics computations on high-quality energy surfaces are presently impossible for molecules of the size considered here, we use reaction path analysis to discuss their possible dynamical behavior.

3.1 Prototype Switcher Based on a "Locked" Polyenal Schiff Base (compound 1). In recent computational work,[34,35,55] it has been shown that PSBs feature nearly competitive photochemical Z/E isomerization paths corresponding to rotary motion about the adjacent double bonds of the chromophore. The existence of competing paths is clearly undesirable. For this reason, **1** represents a good prototype for the design of switchers based on the penta-2,4-dieniminium chromophore. In fact:

(i) five member rings restrain isomerization about the initial −CH=NH− and terminal −CH=CH− double bonds of the structure;

(ii) five member rings are conformationally rigid so that the possible existence of different conformers of the molecule is avoided;

(iii) two −(CH$_2$)$_2$− saturated bridges create a scaffold for functionalization of the switcher and for the introduction of stereogenic centers (see subsection 3.2).

Notice that property (i) is also satisfied by the diarylene light-driven molecular rotor[13−16] mentioned above. However, these molecules have "locks" based on cyclohexenylidene rather than cyclopentenylidene rings and are therefore conformationally less rigid. This flexibility is, in principle, a source of conformational intermediates of the "I" type of Scheme 1b and are therefore undesirable.

While the five-membered ring "locks" of structure **1** are responsible for the favorable properties i-iii, they also introduce an angular (Bayer) strain that modifies the values of the N_1−C_5−C_4 and $C_{1'}$−$C_{2'}$−$C_{3'}$ angles of the penta-2,4-dieniminium moiety. Similarly, the inductive effects due to alkyl substitution at the N_1, C_4, $C_{1'}$, and $C_{3'}$ must change the S_1 and S_0 positive charge distribution along the chromophore framework. In principle, these effects may change the favorable properties of the penta-2,4-dieniminium cation seen in Schemes 2 and 3a. Thus, to assess whether these properties are still satisfied by **1**, we computed the photoisomerization paths for both the *E*-**1** → *Z*-**1** and *Z*-**1** → *E*-**1** processes.

Inspection of Figure 1 indicates that the computed E → Z and Z → E paths conform to the model energy surface of Scheme 3a and, thus, display an energy inflection point in

(55) De Vico, L.; Page, C. S.; Garavelli, M.; Bernardi, F.; Basosi, R.; Olivucci, M. *J. Am. Chem. Soc.* **2002**, *124*, 4124−4134.

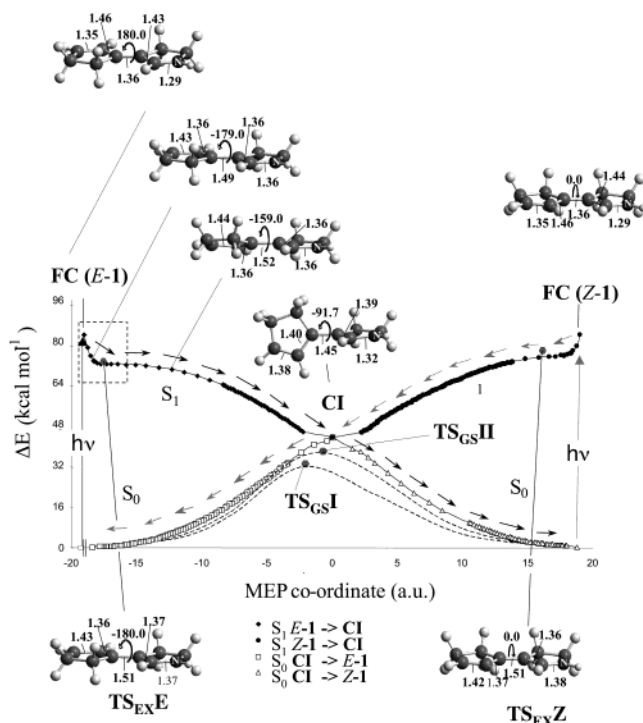**Figure 1.** Energy profiles along the four MEPs describing the relaxation from the **FC** points of the *E*-**1** and *Z*-**1** stereoisomers and their (common) **CI** point. Full and light arrows indicate the E → Z and Z → E photoreaction, respectively. The structures (parameters in Å and degrees) document the molecular structure change along the **FC**(*E*-**1**) → **CI** coordinate. The framed S_1 energy profile is located on an energy surface of the type seen in Scheme 3a. Accordingly, **TS$_{EX}$E** and **TS$_{EX}$Z** correspond to the transition states separating the clockwise and counterclockwise relaxation. **TS$_{GS}$I** and **TS$_{GS}$II** are transition states driving ground state *Z/E* isomerization. The CASSCF S_1 energies of all points along the S_1 and S_0 MEPs have been scaled[69] to match the S_1 CASPT2//CASSCF energies computed for *E*-**1**, *Z*-**1** and **CI**.

correspondence of a change in direction of the reaction coordinate (first dominated by stretching and then by twisting deformations). The fact that the **FC** regions of *E*-**1** and *Z*-**1** have the shape seen in Scheme 3a, is also demonstrated by the existence of two planar S_1 transition states (**TS$_{EX}$E** and **TS$_{EX}$Z**). Notice that the existence of these transition states implies that the energy surface is symmetric with respect to an out-of-plane deformation and therefore S_1 clockwise and counterclockwise twisting motions have the same probability to occur.

For both the E → Z and Z → E paths S_1 → S_0 decay occurs in the region of a conical intersection (**CI**) displaying a ca. 90° central bond. The data of Figure 1 also indicate that, similarly to S_1 relaxation, S_0 relaxation does not involve formation of any intermediate and the system relaxes directly to the energy minimum corresponding to the photoproduct well. Since *Z*-**1** is the photoproduct of *E*-**1** and this is the photoproduct of *Z*-**1**, the two paths in Figure 1 describe *a complete photocycle* leading to a return to the original material after absorption of two photons of similar wavelengths. Finally, notice that two different ca. 90° twisted transition states (**TS$_{GS}$I** and **TS$_{GS}$II**) both controlling *E*-**1** → *Z*-**1** and *Z*-**1** → *E*-**1** thermal isomerization have been located ca. 40 kcal mol^{-1} above the S_0 equilibrium structures. Such barriers guarantee that the thermal isomerization will not compete with the photochemical process in these species. As previously reported[55] the general presence of two different transition states driving the *same* thermal *Z/E* isomerization of a PSBs is a consequence of the fact that the lower

(S_0) tip of the conical intersection splits the ground-state energy surface in two different valleys.

3.2 A Chiral Derivative (compound 5,5′-diMe-1). The comparison of the symmetric energy surface of Scheme 3a with the asymmetric energy surface of Scheme 3b provides a pictorial demonstration that the breaking of the torsional symmetry of the S_1 potential energy surface of **1** must prompt E → Z (for the *E*-**1** isomer) or Z → E (for the *Z*-**1** isomer) unidirectional rotary motion. In these conditions the initial relaxation involves:

(i) immediate coupling of the stretching and torsional coordinate (as the gradient at **FC** will now have a small component along the torsional deformation).

(ii) higher probability of clockwise (or counterclockwise) rather than counterclockwise (or clockwise) motion since the local force field will now be asymmetric with respect to the two directions of torsional deformation.

In principle, such breaking can be induced at **FC** by strategically placed substituents changing **1** to a chiral derivative, such as 5,5′-diMe-**1**.

In Figure 2 we report an analysis of the energy relationship between **FC** (i.e., the *Z*-**1**, 5,5′-diMe-*E*-**1** and 5,5′-diMe-*Z*-**1** equilibrium structures), the S_1 transition structure (i.e., **TS$_{EX}$Z** and **TS$_{EX}$E**) and the conical intersection structures connected to **FC** through clockwise and counterclockwise deformation (**CI** and **CI′** or **CI$_P$** and **CI$_M$**). As expected the **FC**, **TS$_{EX}$Z** structures of *Z*-**1** (see Figure 2a) occurs at 0° torsion and, consistently with Scheme 3a, the two ca. 90° twisted conical intersections, **CI** and **CI′**, are mirror images (i.e., enantiomers). In contrast, the **FC** and **TS$_{EX}$Z** points of structure 5,5′-diMe-*Z*-**1** (see Figure 2b) are displaced from planarity by −2° and −1°, respectively. Consistently with Scheme 3b, the two conical intersections, **CI$_P$** and **CI$_M$**, are not enantiomers but diastereoisomers (also notice the difference in the absolute value of their torsional angles and energies). Similarly, the **FC** and **TS$_{EX}$E** points of structure 5,5′-diMe-*E*-**1** are displaced from planarity (the torsional angles are 174° and −171°, respectively).

Since **TS$_{EX}$Z** defines the lowest energy point along the ridge separating the clockwise and counterclockwise slopes of the S_1 energy surface (see the "ridge" in Scheme 3b), then a molecule relaxing from **FC** will be accelerated toward the steepest slope directing the *Z/E* isomerization motion in a specific direction. For this reason the **R** enantiomer of 5,5′-diMe-*Z*-**1** (that of Figure 2b) is expected to direct the motion toward **CI$_P$** (as pointed out by the arrows). This idea is rigorously demonstrated by computing the initial parts of the excited-state relaxation paths of the E and Z forms of **1** and 5,5′-diMe-*Z*-**1** that are, in fact, pointing toward **CI$_P$**. The corresponding data are given in the Supporting Information.

3.3 Photoisomerization Path of a Synthetically Accessible Derivative (structure 2H). Compounds **1** and 5,5′-diMe-**1** are presently unknown. Thus, while their synthesis represents an attractive research target, the properties predicted above cannot be experimentally assessed. For this reason, we have looked for a analogue that could be synthesized. The synthesis of **2H** has been reported (see below). This compound features the same five-membered heterocycle seen in **1**. However, the cyclopentenylidene ring is replaced with a benzylidene unit. While **2H** features an augmented conformational freedom due to the presence of the unlocked single bond holding the phenyl ring, it represents an analogue of the achiral switcher **1**. We will now
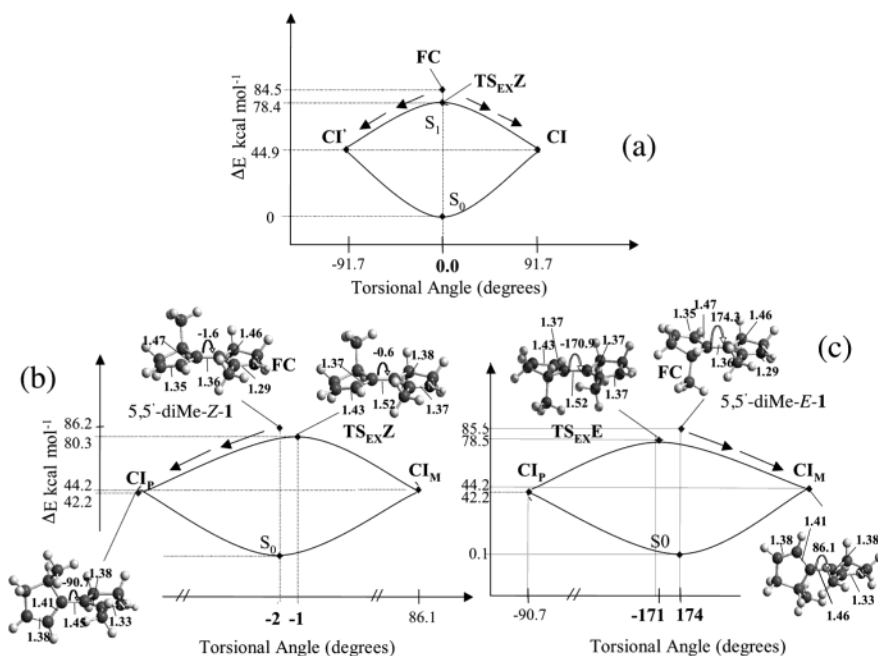
Figure 2. Relationship between relative energy and $C_{1'}-C_4$ torsion for the S_1 stationary points and conical intersections of: (a) Z-**1**, (b) 5,5′-diMe-Z-**1**, and (c) 5,5′-diMe-E-**1**. In **1**, the planar **FC** and **TS$_{EX}$Z** are located at the center of the plot. Clockwise and counterclockwise relaxation lead to two enantiomeric conical intersections, **CI** and **CI′**. In 5,5′-diMe-**1**, **FC** for the Z- and E-stereoisomers, **TS$_{EX}$Z** and **TS$_{EX}$E** are displaced from planarity. Clockwise and counterclockwise relaxation are not equivalent and lead preferentially to one of the two diastereomeric conical intersections **CI$_P$** or **CI$_M$**.

show that, indeed, the electronic and molecular structure of this species presents several of the features seen for **1**.

As displayed in Figure 3, E-**2H** is planar. In contrast Z-**2H** features a 6° twist about the central double bond and a 45° twist about the adjacent unlocked single bond. Presumably, the phenyl ring is twisted out-of-plane by the steric interaction with the heterocycle hydrogen. The corresponding destabilization also accounts for the higher stability (-1.2 kcal mol^{-1}) of E-**2H** with respect to Z-**2H**.

The **TS$_{GS}$I** connecting the two forms features a ca. 80° twisted central double bond, and is located 43.9 kcal mol^{-1} above E-**2H**. Thus, as for compound **1**, such a high barrier indicates that the E- and Z-forms will not thermally interconvert at room temperature.

The excited-state surfaces of **2H** and **1** present remarkable differences. In fact, **2H** has two low-lying $\pi\pi^*$ excited states separated by less than 2 kcal mol^{-1}. At **FC**, the CASSCF level of theory yields a spectroscopic state corresponding to S_2, whereas the lower S_1 state corresponds to a dark state located 2.4 kcal mol^{-1} lower in energy. When dynamic correlation is included, the spectroscopic state is pushed down by 5.3 kcal mol^{-1} (see Figure 3), while the dark state is pushed up by only 0.3 kcal mol^{-1} Thus, at the CASPT2 level, the energy order of the spectroscopic and dark state is inverted. Notice that due to this inversion the S_2/S_1 crossing found at the CASSCF level does no longer occur. Thus, at the CASPT2 level the spectroscopic state is the lowest excited state along the entire reaction coordinate.

The analysis of the computed reaction coordinate reveals some other differences between **2H** and **1**. In particular, the S_1 path features a minimum **MIN$_{EX}$** and a transition state **TS$_{MINEX \to CI}$** (located 1.6 kcal mol^{-1} higher in energy) connecting **MIN$_{EX}$** to a conical intersection **CI$_{S1/S0}$**. Comparison of structures E-**2H** and **MIN$_{EX}$** reveals that, similar to compound **1**, the initial relaxation of the molecule is dominated by a

stretching (the central double bond expands from 1.36 Å to 1.39 Å) coupled with a limited 4° torsional deformation about the central double bond and a 3° deformation about the adjacent unlocked single bond.

The evolution of **MIN$_{EX}$** is dominated by twisting about both the central double bond and the adjacent unlocked single bond. Such deformation causes the hydrogen atom in ortho-position to approach one of the hydrogen atoms placed at C_4 of the pyrroline ring. The distance between these two atoms changes from 2.22 Å at **MIN$_{EX}$** to 2.02 Å in **TS$_{MINEX \to CI}$**. This steric interaction is partially avoided by the twisting of the phenyl ring (3° in **MIN$_{EX}$**, 13° in **TS$_{MINEX \to CI}$**) that slowly returns to planarity once surpassed the transition state. The lowest energy point of the S_1 energy surface corresponds to the conical intersection structure **CI$_{S1/S0}$** featuring a ca. 90° twisted central double bond.[41] Despite the small computed barrier, **TS$_{MINEX \to CI}$** may allow partial or complete energy redistribution at **MIN$_{EX}$**. In practical terms the $\sim$10 kcal mol^{-1} photon energy separating **FC** and **MIN$_{EX}$** may be, at least partially, redistributed. Thus, the photoisomerization path of E-**2H** may be consider closer to that given in Scheme 1b due to the presence of a transient I* corresponding to **MIN$_{EX}$**. In contrast, we have not been able to locate any intermediate I along the S_0 relaxation path.

To assess if structure **2H** could be used as the basic chromophore for the development of a single-molecule rotor analogue to 5,5′-diMe-**1**, we have investigated the **R** enantiomer of the chiral structure 4-Me-E-**2H** where a methyl group has been inserted at C_4. Although the computation of the full photoisomerization path of 4-Me-E-**2H** goes beyond the scope of the present work an analysis of its optimized S_0 structure reveals a firm deviation from planarity. In fact, the dihedral angle between the planes defined by the two cycles has a value of 4.4°, whereas the phenyl plane is twisted by 17.4° with respect to the central double bond. This structural deformation
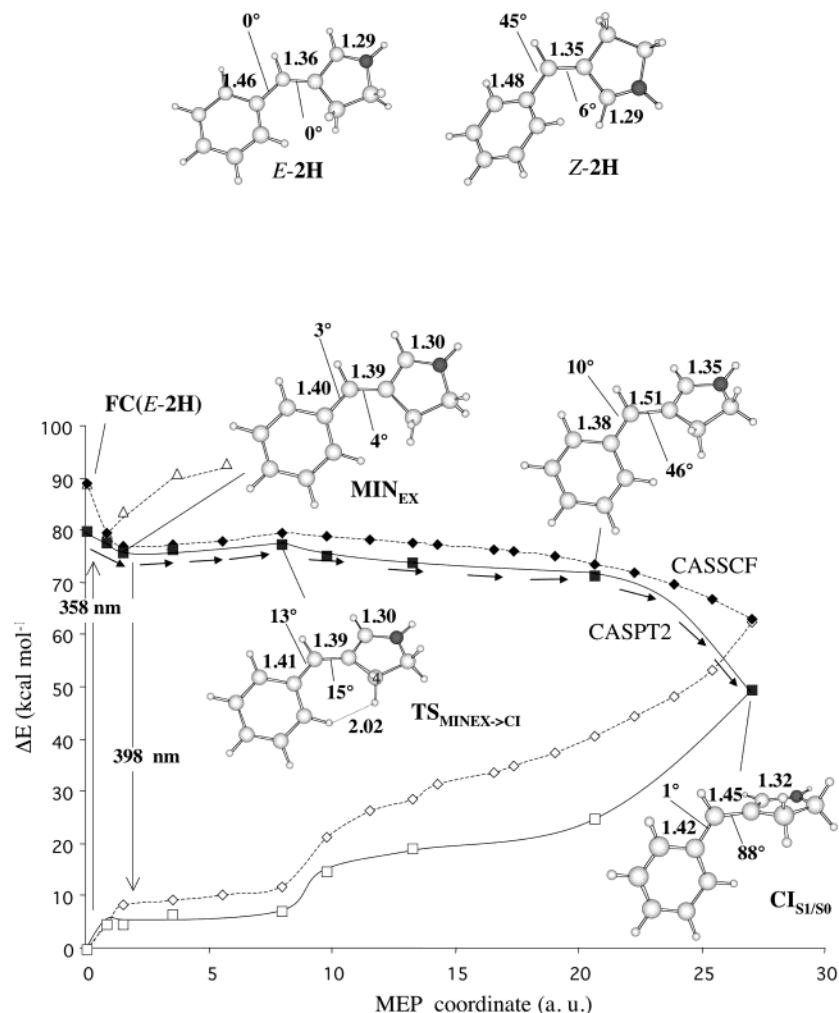
Figure 3. Energy profiles along the MEP describing the excited-state relaxation $(\text{FC}(E\text{-}2H) \rightarrow \text{MIN}_{EX} \rightarrow \text{TS}_{\text{MINEX}\rightarrow\text{CI}} \rightarrow \text{CI}_{S1/S0})$ of E-**2H**. Full and open diamonds indicate the CASSCF S_1 and S_0 energies, respectively; full and open squares indicate the CASPT2 S_1 and S_0 energies; open triangles indicate the CASSCF S_2 energies. The structures (geometrical parameters in Å and degrees) document the progression along this path and the equilibrium structures of the E-**2H** and Z-**2H** stereoisomers.

is consistent with a helical structure of the molecule that suggests a S_1 potential energy surface of the type seen in Scheme 3b.

3.4 Syntheses of the Neutral Imines 2neut, *p*-MeO-2neut, *p*-NO₂-2neut. The search for synthetically available molecules containing the penta-2,4-dieniminium unit, led us to select the 3-alkylidene-1-pyrrolines, for which a number of synthetic methods[56-61] have been reported to date. In particular, in the first phase of the project, we turned our attention to simple para-substituted-3-benzylidene-1-pyrrolines whose structures incorporate the crucial part of the wanted π-conjugated system and allow for a change in the nature of the para-substituent on the phenyl ring that could be used to adjust the electron density within the π-system. (As we will discuss below, this simple modification has also been exploited to "tune" the photochemical behavior of these molecules.)

Most of the synthetic approaches to these targets feature a cationic cyclization[58-61] as the key step even if, at least in

principle, they could result from an aldol-like condensation between 1-pyrroline and appropriate aldehydes. This last approach seemed to us the preferable route since it leads to the target compounds in a straightforward way, although, due to its tendency to trimerize, the material referred to as 1-pyrroline[62] presents special difficulties in the isolation.[62-65] (In no case a suitable method for isolation of 1-pyrroline in pure form was developed.)

In 1982, it was developed a more convenient route to 1-pyrroline trimer by silver (I) catalyzed oxidation of pyrrolidine with peroxodisulfate and, for the first time, it could be unambiguously assigned the structure of 1,6,11-triazatetracyclo-[10.3.0.0.²,⁶0⁷,¹¹]pentadecane[66] (see Scheme 4). Interestingly, the same authors found that this material reacted with benzaldehyde to furnish 3-benzylidene-1-pyrroline **2neut** in acceptable yield.[67]

(56) Meyers, A. I.; Ritter, J. J. *J. Org. Chem.* **1958**, *23*, 1918−1922.
(57) Sugasawa, S.; Ushioda, S. *Tetrahedron* **1959**, *5*, 48−52.
(58) Gawley, R. E.; Termine, E. J. *J. C. S. Chem. Commun.* **1981**, 568−569.
(59) Sakane, S.; Matsumura, Y.; Yamamura, Y.; Ishida, Y.; Maruoka, K.; Yamamoto, H. *J. Am. Chem. Soc.* **1983**, *105*, 672−674.
(60) Gawley, R. E.; Chemburkar, S. *Tetrahedron Lett.* **1986**, *27*, 2071−2074.
(61) Gawley, R. E.; Chemburkar, S. *Heterocycles* **1989**, *29*, 1283−1292.

(62) Fuhlhage, D. W.; Vander Werf, C. A. *J. Am. Chem. Soc.* **1958**, *80*, 6249−6254.
(63) Cragg, J. E.; Herbert, R. B.; Jackson, F. B.; Moody, C. J.; Nicolson, I. T. *J. Chem. Soc, Perkin Trans. 1* **1982**, 2477−2485.
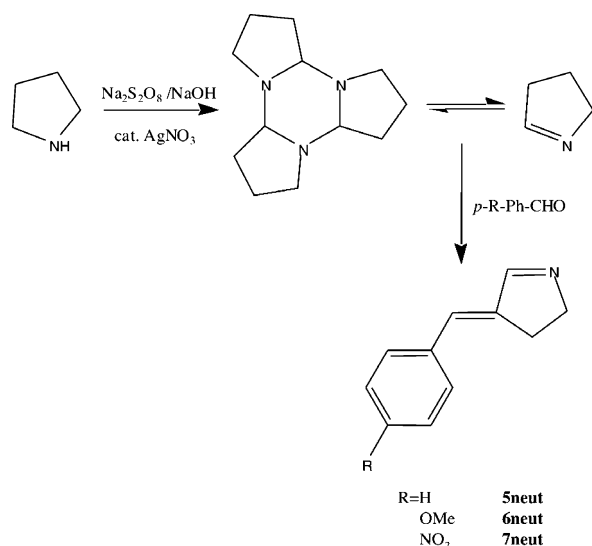(64) Jakoby, W. B.; Fredericks, J. *J. Biol. Chem.* **1959**, *234*, 2145−2150.
(65) Richards, J. C.; Spenser, I. D. *Tetrahedron* **1983**, *39*, 3549−3568.
(66) Ogawa, K.; Nomura, Y.; Takeuchi, Y.; Tomoda, S. *J. Chem. Soc., Perkin Trans. 1* **1982**, 3031−3035.
(67) Nomura, Y.; Bando, T.; Takeuchi, Y.; Tomoda, S. *Bull. Chem. Soc. Jpn.* **1983**, *56*, 3199−3200.

Scheme 4

They showed how the predominant trimer has to be in equilibrium with 3,4-dihydro-2-*H*-pyrrole, that is in turn able to react with benzaldehyde in an aldol-like condensation. The main advantage of this reaction is the possibility of carrying out the synthesis of the target molecules without the use of any basic or acid catalysts, a need due to the extreme chemical instability of 1-pyrroline.[62]

The application of this protocol led us to obtain the unknown derivatives *p*-MeO-**2neut** and *p*-NO$_2$-**2neut** simply by combining the trimer with *p*-methoxy- or *p*-nitro benzaldehyde, respectively. However, in the latter case, adopting usual reaction conditions, only traces of the desired *p*-nitro benzylidene derivative are formed; instead, a solid and unexpectedly polar compound (TLC) is dominant in the reaction mixture. Due to the lack of olefin proton signal on the 1H NMR spectrum this was tentatively assigned to the intermediate aldolic reaction product. Consequently, we decided to force the removal of water by heating a methanolic solution of this intermediate in the presence of AcOH/AcONa buffer, furnishing the desired compound in more than 40% yield.

In all cases, the preparations of **2neut**, *p*-MeO-**2neut**, and *p*-NO$_2$-**2neut** yielded a major E-stereisomer and only minor quantities of the Z-stereisomer. The geometry of their exocyclic double bonds was easily inferred both on the base of characteristic[53] coupling between allylic methylene protons and the exocyclic olefin protons and, on NOE experiments. It is noteworthy that the E isomers partially convert to Z isomers by the action of UV light and that by chromatography we could separate the diastereisomers eventually transformed to the targeted E- and Z-isomers of imines **2**, *p*-MeO-**2**, and *p*-NO$_2$-**2** (see Supporting Information).

3.4.1 Absorption Spectra. The synthesis of **2H** allows the validation of our computational strategy (see subsection 2.1) by comparing computed (gas-phase) and measured (solution) spectroscopic quantities such as the absorption maximum (λ_{max}). As reported in Table 1 we observed two main bands (see the spectrum of **2H** in Figure SI4 of the Supporting Information) with λ_{max} at 225 nm and at 326 nm, respectively.

The long wavelength band in the recorded spectrum can be related to the computed S$_0$ → S$_1$vertical transition. This transition has a λ_{max} = 358 nm with an oscillator strength of 0.82, whereas

Table 1. UV/Vis Absorptions (λ_{Max}) of Compounds **2**, *p*-MeO-**2**, and *p*-NO$_2$-**2**

structure	λ_{max}, nm	ϵ, M^{-1}cm^{-1}	λ_{max}, nm	ϵ, M^{-1}cm^{-1}
E-**2H**	326	30600	225	10300
Z-**2H**[a]				
E-**2**	327	17400	254	26000
Z-**2**	328	11800	248	21000
p-MeO-*E*-**2**	364	6600	265	10100
p-MeO-*Z*-**2**	365	6600	265	13600
p-NO$_2$-*E*-**2**[b]	322	13000	223	8500
p-NO$_2$-*Z*-**2**[b]	310	19000	224	18000

[a] Unstable. [b] Introduction of EW−NO$_2$ in compound **2** results in a relatively small difference in the UV/Vis absorption spectra for the *Z*- and *E*-isomers. In fact *p*-NO$_2$-*E*-**2** absorbs at λ_{max}=322 nm (ϵ=1300) and *p*-NO$_2$-*Z*-**2** has a higher-intensity absorption at 310 nm (ϵ=1900).

the experimental absorption has a maximum at 326 nm, with an approximate oscillator strength of 0.7. Although S$_2$ was found to be nearly degenerate to S$_1$, it has *f* = 0.029. The S$_0$ → S$_2$ transition is thus expected not to contribute to the qualitative aspect of the spectrum since the corresponding weak band will be hidden by the close and intense band associated with the first transition. For the S$_0$ → S$_3$ transition we compute a λ_{max} value of 253 nm with an oscillator strength of 0.16. This values compare reasonably well with the observed λ_{max} = 225 nm and *f* = 0.1.

The computed spectra are found to be red-shifted with respect to the spectral bands observed in acetonitrile. The deviation between the theoretical results and the experimental data −0.34 eV for the S$_0$ → S$_1$ transition and −0.61 eV for the S$_0$ → S$_3$ transition) is larger than the expected CASPT2 error (typically 0.2 eV) on excitation energies. Furthermore, we find that the vertical excitation energy values obtained using the 6-31+G* basis set are very close to those computed with the 6-31G* basis set (see Table SI2 in the Supporting Information) supporting a very limited basis set effect. We conclude that the observed deviation is most probably due to the effect of the (solvated) negative counterion present in solution on the different electronic structure (charge distribution) of the ground and excited states of **2H**. In fact, as previously reported,[43] the S$_1$ state of the penta-2,4-dieniminium chromophore has a dominant charge-transfer (i.e., ionic) character while the S$_2$ state has a diradical (i.e., covalent) character. Due to the more extended π-system (i.e., a phenyl group is replacing a double bond) the S$_1$, S$_2$, and S$_3$ states of **2H** all feature a charge-transfer character that can be quantified in terms of the total charge of the benzylidene and heterocyclic moieties (see the Supporting Information for the details). Accordingly, the main resonance formulas describing these states are as follows:
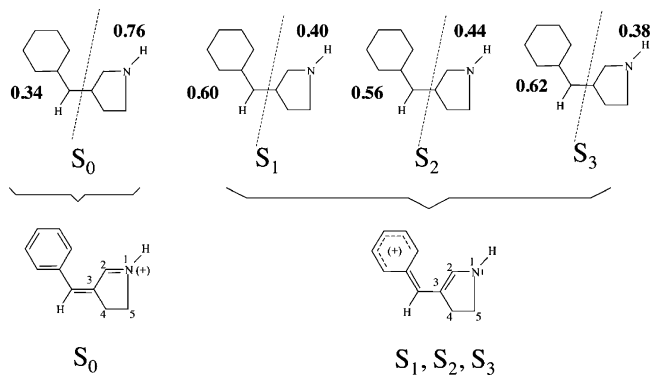
In solution, the counterion will be statistically closer to the locus of the positive charge of the S_0 structure (i.e., the $-CH=NH-$ moiety). Upon $S_0 \rightarrow S_1$ excitation the positive charge is translocated in the region of the phenyl ring and therefore away from the counterion. It is therefore clear that, in the presence of the counterion the S_0-S_1 energy gap will increase due to preferential stabilization of S_0 relative to S_1 yielding a blue-shifted λ_{max}. The same reasoning leads to the conclusion that also the S_0-S_3 energy gap will be increased by the presence of the counterion.

The spectra of **2**, *p*-MeO-**2** and *p*-NO$_2$-**2** have the same two-band structure characterizing the spectrum of the parent compound **2H**. The comparison between the spectroscopic data for **2H** and **2** shows virtually no differences regarding the first photoactive band, which occurs at an almost identical wavelength in the two compounds ($\lambda_{max} = 326$ nm in **2H** compared $\lambda_{max} = 327$ nm in **2**). These results suggest that the excited-state behavior of **2** and **2H** will be substantially equal. Accordingly, below we focus exclusively on the more experimentally tractable methylated compound **2** and its derivatives.

The data in Table 1 shows that, for both the E- and Z-stereoisomers, the λ_{max} values of the first and second band are sensitive to the electron-withdrawing (EW) or electron-releasing (ER) character of the substituent in para-position. In compound *p*-MeO-**2** that carries an ER group the two bands are red-shifted relative to **2**, while in compound *p*-NO$_2$-**2** that instead carries the EW group they are blue-shifted. These spectral changes are, again, readily explained on the basis of the electronic structure of the S_0, S_1, and S_3 states. Accordingly, the ER groups (e.g., $-OCH_3$) that stabilize the phenyl ring positive charge will stabilize the S_1 and S_3 state relative to the S_0 state leading to a red-shifted λ_{max} of the first and second band. In contrast, the EW groups (e.g., $-NO_2$) that destabilize the positive charge on the phenyl ring will yield blue-shifted λ_{max}. The comparison of the spectra for *p*-MeO-**2** and *p*-NO$_2$-**2** with that of **2** is thus fully consistent with the computed S_3, S_1, and S_0 electronic structures.

3.4.2 Photoisomerization and Composition of the Photostationary States. According to the reaction path of Figure 3, upon irradiation *E*-**2** is expected to produce *Z*-**2**. Similarly *Z*-**2** is expected to produce *E*-**2**. Because these species have comparable λ_{max} and ϵ values, one expects generation of a photostationary state (PPS) whose composition (i.e., ratio between the E- and Z-forms) is independent from the starting stereoisomer and controlled by the differences in *Z*-**2** and *E*-**2** extinction coefficients and by the differences in quantum yields of the $Z \rightarrow E$ and $E \rightarrow Z$ photoreactions. Indeed, Pyrex-filtered irradiation of both *Z*-**2** and *E*-**2** yielded after 1−2 h fully equivalent mixtures of both stereoisomers in a 3:1 ratio (determined via ^{1}H NMR), always with the E form as the main product. This fact corroborates that *Z*-**2** is the photoproduct of *E*-**2** and, in turn, this is the photoproduct of *Z*-**2**. Thus, consistently with the mechanism shown in Figure 1 for the simpler chromophore **1**, irradiation of **2** must lead to a *photocycle*.

The basic photocycle proposed for our class of switchers implies that, at a given wavelength, the differences in extinction coefficient (roughly, the differences in absorption maxima) of the Z and E forms can be exploited to control the PPS composition. Thus, to support the computed mechanism, we

Table 2. PSS Composition for Compounds **2**, *p*-MeO-**2**, and *p*-NO$_2$-**2**

compound	λ (nm)	ratio[a] at PSS	
		E	Z
2	313	1	0.3
p-MeO-**2**	313	1	0.1
p-NO$_2$-**2**	313	1	1
p-NO$_2$-**2**	300	1	0.1
p-NO$_2$-**2**	310	1	0.7
p-NO$_2$-**2**	320	1	1
p-NO$_2$-**2**	330	1	1
p-NO$_2$-**2**	360	1	1.5
p-NO$_2$-**2**	223	1	0

[a] Ratios determined by ^{1}H NMR peak integral.

investigate the substituent and wavelength dependence of the PPS. The effect of the substituent was investigated using a fixed irradiation wavelength ($\lambda_{max} \geq 313$ nm) for **2**, *p*-MeO-**2** and *p*-NO$_2$-**2**. Although compound **2** showed a 3:1 ratio with *E*-**2** as the main product, the ratio for *p*-MeO-**2** was raised to 10:1 and for *p*-NO$_2$-**2** was 1:1. This effect cannot be explained only on the basis of different values of the λ_{max} as in **2** and *p*-MeO-**2** these values are substantially identical for the E and Z forms (see Table 1). Nevertheless, with respect to the unsubstituted compound, the ER substituent of *p*-MeO-**2** induces a shift of the composition toward the E-form. This implies that the quantum yields for the $E \rightarrow Z$ and $Z \rightarrow E$ processes depend on the substituent and that the $Z \rightarrow E$ process is enhanced by the $-OCH_3$ group. Such complex effects cannot be explained on the basis of qualitative considerations and require further computational/mechanistic studies to be correctly interpreted.

According to Table 1 compound *p*-NO$_2$-**2** features slightly different long-wavelength λ_{max} for the E- and Z-forms. Thus in this compound one would predict a sensitivity of the PPS composition to the irradiation wavelength. In fact, our experimental data (see Table 2) show that, increasing the wavelength from 300 to 360 nm, the PPS E/Z ratio inverts from 1:0.1 to 1:1.5. (i.e., from 91% *p*-NO$_2$-*E*-**2** and 9% *p*-NO$_2$-*Z*-**2** to 40% and 60%, respectively).

As mentioned in Section 3.4.1, our compounds present a second band at ca. 225 nm assigned to the $S_0 \rightarrow S_3$ transition. We selectively irradiated this band in *p*-NO$_2$-*E*-**2**. After several hours of irradiation at 223 nm no traces of the Z-isomer could be found. However, irradiation of the Z-isomer in the same band yielded the more stable E-isomer with complete conversion. Since no side-reaction disrupting the photocycle could be detected, this result suggests that photoisomerization from S_3 follows a different (but well defined) reaction pathway involving three excited-state energy surfaces. The computational investigation of such complex pathway goes beyond the scope of the present work.

Notice that the degree of photodegradation of **2** (a property of great importance for the applications of molecular switchers) was assessed irradiating the photostationary mixture for 24 h in the same reaction conditions. We found that the ^{1}H NMR spectrum remained unaltered after that time, showing that the photochemical decomposition of these molecules is minimal.

3.4.3 Photophysical and Photochemical Properties of *p*-NO$_2$-2. To elucidate the S_1 deactivation mechanism of the compounds under investigation and to collect quantitative information about the quantum efficiency of the photoreaction, we carried out a photophysical study of *p*-NO$_2$-**2** including flash-
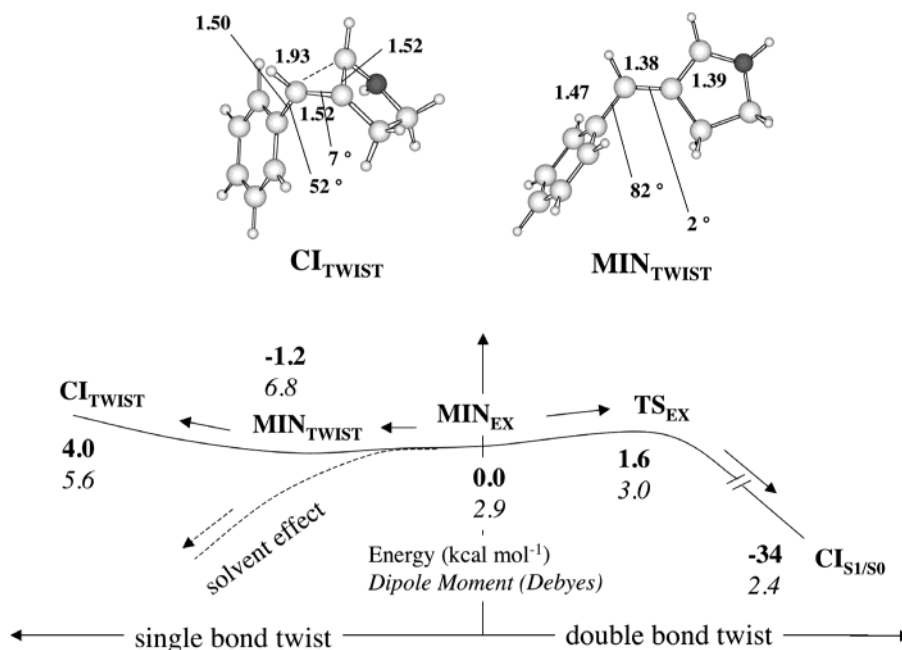
Figure 4. S_1 reaction paths controlling the evolution and decay of **2H**. The $\mathbf{MIN_{EX}} \rightarrow \mathbf{TS_{MINEX \rightarrow CI}} \rightarrow \mathbf{CI_{S1/S0}}$ path is documented in Figure 3. The $\mathbf{MIN_{EX}} \rightarrow \mathbf{MIN_{TWIST}} \rightarrow \mathbf{CI_{TWIST}}$ is associated with rotation about the single-bond connecting the phenyl moiety to the central double bond. The bold numbers along the energy profile document the relative change in energy. The numbers in *italic* document the change in molecular dipole moment. The structures (parameters in Å and degrees) document the progression along the single bond twisting path.

photolysis experiments with ns-resolution. In this section, we report the preliminary results of such investigation. First of all, no effective radiative decay channel seems to be operative in *p*-NO$_2$-*E*-**2** and *p*-NO$_2$-*Z*-**2** in acetonitrile solutions as demonstrated by the absence of fluorescence emission in the UV−vis region. Taking into account the instrumental sensitivity, an upper limit of 10^{-4} was estimated for the fluorescence quantum yields of the two isomers. Upon laser excitation at 355 nm of *p*-NO$_2$-*E*-**2** in acetonitrile solutions at room temperature, no transients were detected in the investigated UV−vis region (300−750 nm) by ns-laser flash photolysis experiments. On the basis of this experiment the presence of either an excited-state or a ground-state intermediate with lifetimes above 20 ns can be excluded. The E → Z photoisomerization process was spectrophotometrically followed in acetonitrile solutions by irradiation of the *p*-NO$_2$-*E*-**2** at 320 and 360 nm. Small E → Z photoisomerization quantum yields (ca. 6×10^{-3}) were measured in these experimental conditions indicating that the majority of the lowest excited state (S$_1$) population does not decay through the Z/E reactive channel.

The facts that *p*-NO$_2$-*E*-**2** does not show any fluorescence and no long-lived excited- or ground-state transients are detected are consistent with the photoisomerization path presented in Figure 3 (the only source of fluorescence may be $\mathbf{MIN_{EX}}$. However, even a simple Arrhenius picture of its decay via $\mathbf{CI_{S1/S0}}$ would yield an excited-state lifetime of ca. 2 ps that is well below our 20 ns resolution). In contrast, the observed very limited *p*-NO$_2$-*E*-**2** → *p*-NO$_2$-*Z*-**2** quantum yield is at variance with the proposed *gas-phase* mechanistic picture. Indeed, decay at a 90° twisted conical intersection located at the very bottom of the S$_1$ energy surface should lead to an efficient photoisomerization with a quantum yield >0.5. For this reason, we shall conclude that, in the chosen experimental conditions, *p*-NO$_2$-*E*-**2** must decay via an *unreactive* channel. The nature of this channel was investigated via further mapping of the S$_1$

energy surface of the parent system **2H**. As reported in Figure 4 the calculations revealed that a flat conformational path exists along the unlocked single bond torsion leading to a new excited-state intermediate ($\mathbf{MIN_{TWIST}}$) featuring a ca. 90° twisted phenyl ring and lying 1.2 kcal mol^{-1} below $\mathbf{MIN_{EX}}$. Most importantly a new conical intersection ($\mathbf{CI_{TWIST}}$) structure connected to $\mathbf{MIN_{TWIST}}$ was located ca. 4 kcal mol^{-1} higher in energy than $\mathbf{MIN_{EX}}$. Inspection of the $\mathbf{CI_{TWIST}}$ structure (close to that documented for polyenes[68]) reveals that despite the highly distorted hetherocycle the double bond is still substantially planar while the single bond features a large twisting. As a result decay at $\mathbf{CI_{TWIST}}$ may only lead to production of a "degenerate" photoproduct, in the sense that twisting about the single bond will only regenerate the starting material.

In the gas phase, the $\mathbf{MIN_{EX}} \rightarrow \mathbf{MIN_{TWIST}} \rightarrow \mathbf{CI_{TWIST}}$ channel is predicted to be less efficient than the $\mathbf{MIN_{EX}} \rightarrow \mathbf{TS_{EX}} \rightarrow \mathbf{CI_{S1/S0}}$ channel due to a ca. 2 kcal mol^{-1} larger energy barrier. Accordingly the discovery of such an alternative decay route is, again, not consistent with a low E → Z quantum yield. However, the computations also reveal that the change in dipole moment occurring along $\mathbf{MIN_{EX}} \rightarrow \mathbf{MIN_{TWIST}}$ should favor population of this route when the molecule is embedded in a polar environment. Indeed, as reported in Figure 4, twisting about the single bond yields a 4 D increase of the dipole moment while twisting about the double bond does not lead to a substantial dipole moment change. The low quantum yield measured in acetonitrile is thus consistent with a >2 kcal mol^{-1}

(68) Celani, O.; Garavelli, M.; Ottani, S.; Bernardi, F.; Robb, M. A.; Olivucci, M. *J. Am. Chem. Soc.* **1995**, *117*, 11 584−11 585.
(69) The energies along the S$_1$ **FC**(*E*-**1**) → **CI** and **FC**(*Z*-**1**) → **CI** MEPs are two-root (S$_0$, S$_1$) state average CASSCF energies relative to the S$_0$ energy of **FC**(*Z*-**1**). The S$_0$ energies along the **CI** → *Z*-**1** and **CI** → *E*-**1** MEPs are single-root (S$_0$) CASSCF energies relative to the S$_0$ energy of **FC** (*Z*-**1**) S$_0$. These relative S$_0$ and S$_1$ energies have been scaled to match the CASPT2 S$_0$ → S$_1$ vertical energy separation at **FC**(*Z*-**1**). The energies of S$_0$ and S$_1$ transition structures are instead true CASPT2 energies (see Table SI2 in Supporting Information).

stabilization of the single bond twisting route and therefore with a strong decrease of the E $\rightarrow$ Z isomerization quantum efficiency. While further computational and, in particular, experimental investigations are required to confirm the existence of the competitive decay pathway illustrated above, it is likely that the synthesis of "single bond locked" derivatives such as **3** should yield compounds displaying highly efficient Z $\rightarrow$ E photoisomerization. Such synthesis is currently pursued in our laboratory.

3
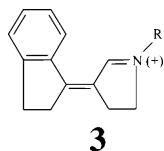
4. Conclusions

Despite the increasing interest in the development of novel and more effective light-driven molecular devices, ab initio quantum chemical methods have not been routinely employed for the design of these functional materials. Among other reasons, the specialized methods required for the correct investigation of excited states, where the photon energy is initially stored, have precluded such a desirable development. Above, we have presented the result of a computational exercise employing state-of-the-art quantum chemical methods such as ab initio CASSCF and CASPT2. The results provide the basis for the development of a class of biomimetic switchers related to the retinal protonated Schiff base chromophore of rhodopsin proteins. In particular, the structure of the photoisomerization paths of the prototype compounds **1** and 5,5′-diMe-**1** satisfy the criteria required for an efficient molecular switcher and motor, respectively. In turn, the successful synthesis and photochemical characterization of three different analogues of **1** (i.e., **2**, *p*-MeO-**2**, *p*-NO$_2$-**2**) clearly call for an increased research effort based on tightly coupled computer modeling and lab synthesis work.

Supporting Information Available: (i) Computational details. (ii) Comparison between E $\rightarrow$ Z and Z $\rightarrow$ E photoisomerization energy profiles for compounds **1** and 5,5′-diMe-**1**. (iii) Comparison between CASSCF and CASPT2 energy profiles for 2H. (iv) Cartesian coordinates for compounds **1**, 5,5′-diMe-**1**, and **2H**. (v) Charge distribution and dipole moments for different structures of compound **2H**. (vi) Full synthetic procedures and photochemical characterization data for compounds **2**, *p*-MeO-**2**, and *p*-NO)-**2**. This material is available free of charge via the Internet at http://pubs.acs.org.

JA038859E